J. Fluid Mech. (1981), *vol.* 113, *pp.* 1–21
Printed in Great Britain

Penetrative convection at low Péclet number

By RICHARD A. DENTON† AND IAN R. WOOD
University of Canterbury, Christchurch, New Zealand

(Received 2 May 1979 and in revised form 3 March 1981)

A theoretical one-dimensional model of penetrative convection in a stable temperature stratification heated from below has been developed in which the partial derivatives of temperature with respect to height and time are assumed to be discontinuous at the interface. As a finite temperature gradient then exists immediately above the interface, molecular diffusion effects at low Péclet number can be included. The results of the numerical-analysis model are used to illustrate the relative contributions of molecular diffusion, interfacial turbulence and the 'filling' of the existing temperature stratification by the lower boundary heat flux. Data from low-Péclet-number experiments are used to verify the results of the theoretical model.

1. Introduction

Two examples of penetrative convection are the growth of a turbulent atmospheric boundary layer during early morning heating in the absence of wind, and the deepening of the surface layer in a large deep power station cooling pond. Both are important in view of present-day environmental problems. The dispersal of pollutants released into the atmosphere will depend on the rate of growth of the boundary layer. Similarly penetrative convection in a cooling pond will affect the heat loss from the warm inflow and, hence, the power station efficiency. The present work has arisen from an investigation of this latter problem.

A major difference between the two examples is the role of molecular diffusion, as expressed by the Péclet number

$$Pe = l_s v_s / \kappa, \tag{1}$$

where l_s and v_s are turbulent length and velocity scales and κ is molecular diffusivity. Following Deardorff (1970) the velocity and length scales may be written as

$$l_s = c_1 d_m, \quad v_s = c_2[\alpha g Q_p l_s]^{\frac{1}{3}}, \tag{2}$$

where d_m is the mixed layer depth, Q_p is the boundary heat flux and $\alpha = -\rho^{-1}\partial\rho/\partial T$ is the volumetric coefficient of thermal expansion.

It will be shown later that, to fit the experimental results, c_1 and c_2 have values of approximately 0·1 and 0·56 respectively. Using these values the Péclet number Pe in the atmosphere, because of the large depth scale, is of the order 10^6. Hence the molecular diffusion is negligible and in atmospheric models it has been assumed that there is a sharp discontinuity of temperature at the inversion.

In a cooling pond the buoyancy heat flux and the thickness of the mixed layer are much smaller. Typically Péclet numbers will be of the order 10^2–10^3 and in this case

† Present address: Sonderforschungsbereich 80, University of Karlsruhe, 7500 Karlsruhe, West Germany.

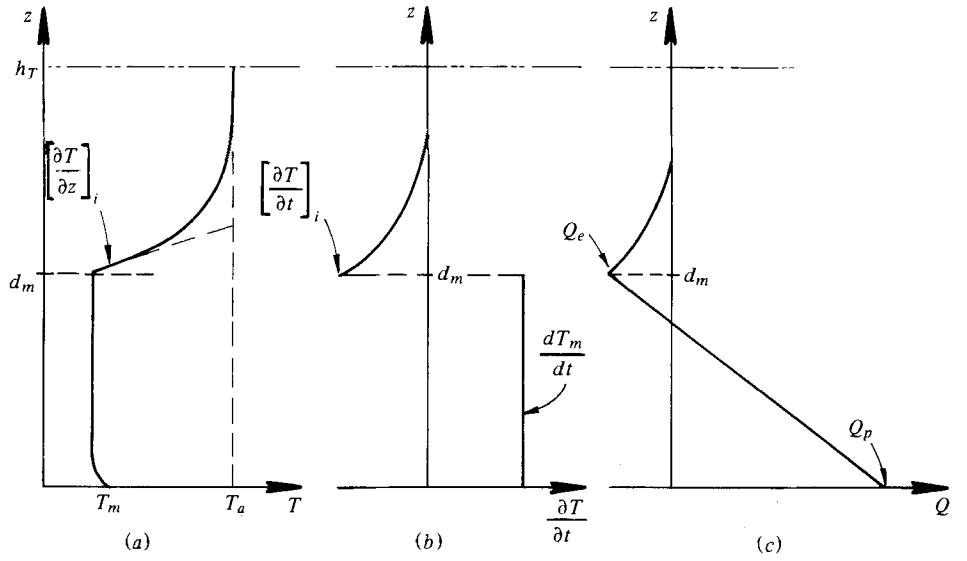

FIGURE 1. (*a*) Idealized vertical temperature profile for penetrative convection and corresponding profiles of (*b*) rate of change of temperature and (*c*) vertical buoyancy heat flux.

molecular diffusion will play a significant role. When considering these low-Péclet-number problems, a sharp interface is not reasonable and the present analysis is a first attempt to overcome this deficiency by assuming a vertical temperature profile which has no discontinuity at the interface.

Instead, the partial derivatives with respect to height and time, $\partial T/\partial z$ and $\partial T/\partial t$, will be taken as discontinuous. The finite temperature gradient above the interface allows molecular diffusion effects to be included (figure 1). The corresponding vertical heat-flux profile includes the heat flux above the interface (figure 1*c*). In Betts's (1973) model this heat flux was zero. To be consistent with the cooling-pond problem the temperature gradient well above and below the interface is zero in the present model.

The large number of experimental and theoretical penetration-convection models which appear in the literature may be categorized into two groups depending on the method used to present the negative interfacial heat-flux Q_e data. For models based on Betts (1973) there is a temperature jump ΔT_i at the inversion so that

$$Q_e = -v_e \Delta T_i, \tag{3}$$

where v_e is the rate of rise of the interface. The energy used at the interface for entrainment is assumed to be a constant fraction of the energy input, in this case the lower boundary heat flux, such that

$$Q_e = -kQ_p. \tag{4}$$

Simplifying the convection-layer heat budget using these two equations yields a relationship for ΔT_i as a function of k, the stable linear gradient Γ above the interface and mixed-layer depth d_m. Comparison with experimental data yields a value for k. A recent review by Stull (1976) gives the mean range of k from field, laboratory and numerical model data as $0{\cdot}1 < k < 0{\cdot}3$, although values well outside this range have been reported.

The second group are the grid-stirring experiments of Rouse & Dodu (1955),

Turner (1968), Wolanski & Brush (1975) and others. Here the interfacial heat flux is non-dimensionalized by the product of the turbulent velocity scale v_s and ΔT_i and expressed as a function of Richardson number defined by $\alpha g \Delta T_i l_s / v_s$ and Pe. For a saline stratification, high Pe, Turner (1968) found $E \sim Ri^{-\frac{3}{2}}$, while for temperature stratification, low Pe, $E \sim Ri^{-1}$. As the Péclet number decreases, the thickness of the interfacial region between the two stirred layers increases until at low Pe a non-turbulent diffusive core exists (Crapper & Linden 1974).

A number of laboratory experiments of penetrative convection have been reported where a linear or two-layered stratification is heated from below (Deardorff, Willis & Lilly 1969; Heidt 1977; Willis & Deardorff 1974; Denton & Wood 1974). Cooling water below its maximum density temperature of 4 °C also produces convective motion at the base of a water column but in this case leads to steady-state penetrative convection (Townsend 1964; Adrian 1975). Penetrative convection at the surface of lakes below the maximum density temperature has been reported by Farmer (1975).

2. The computational model

The penetrative convection system to be analysed is a two-layered temperature stratification heated from below. Inverting the cooling-pond situation simplifies the experimental investigation without altering the physics of the problem (Denton 1978). The temporal behaviour of the model consists of three stages. Only the intermediate stage when the convection layer is created by lower boundary heating and grows by interfacial entrainment will be considered. Solutions for the initial stage prior to heating, when only molecular diffusion is acting to distribute heat throughout the fluid column, and the final stage, when the whole fluid column is convectively mixed, are straightforward.

To understand the interfacial entrainment process, one must first consider the heat-transfer process at the heated lower boundary. Following the phenomenological theory of Howard (1964), the thermal convection process may be considered as the periodic buildup of a molecular diffusion boundary layer and its subsequent breakup due to buoyant instabilities. This process can be visualized with dyed fluid at the lower heated boundary (Sparrow, Husar & Goldstein 1970; Denton 1978). This is best illustrated by considering continuous temperature records from fixed heights within the fluid column (figure 2). A temperature probe just above the heated boundary will measure the buildup of temperature by molecular diffusion and then either a pulse of warmer or colder temperature depending on whether the probe is in the ascending or descending portion of the overturning boundary-layer breakup (figure 2*a*). As rising thermals pass a probe within the convectively mixed layer a positive temperature pulse is recorded (figure 2*b*).

Upon reaching the stable density gradient at the top of the mixed layer the thermals overshoot (Stull 1973). They become denser than their surroundings, are brought to rest and then forced back towards the mixed layer. If a penetrating thermal impinges upon a probe placed just above the interface the continuous temperature output at first registers a rapid decrease in temperature (figure 2*c*) then the damped oscillation of a forced gravity wave on the stable density gradient. Beyond the penetration distance of the thermals but in a region of stable density gradient the regular oscillation of

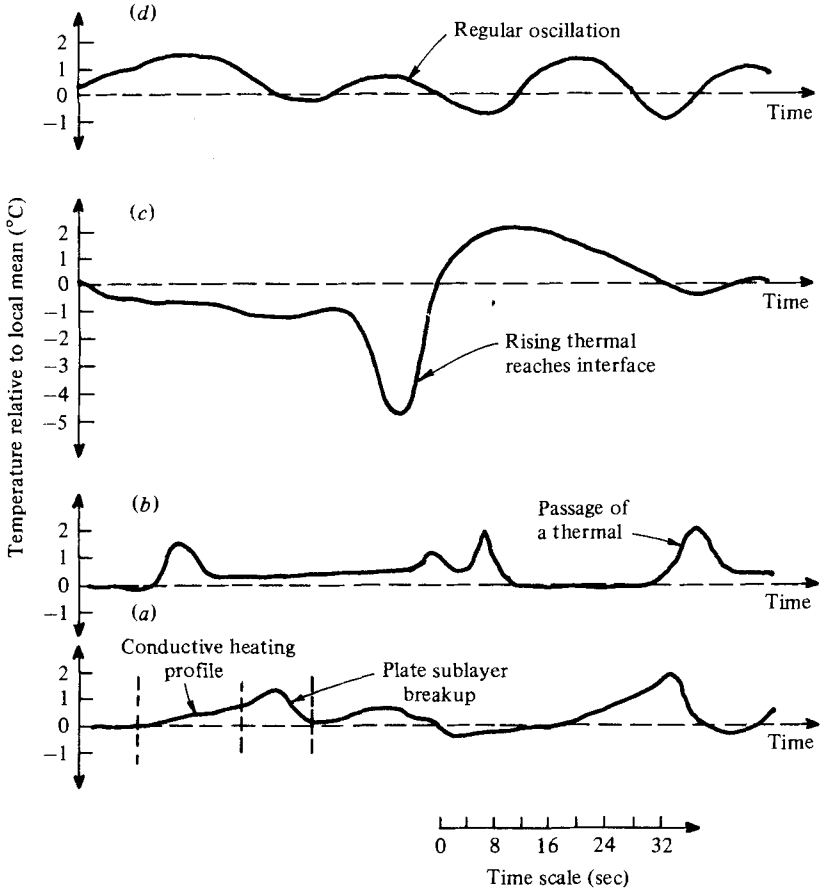

FIGURE 2. Continuous temperature data from four fixed heights within the fluid column. As the measurements were not taken simultaneously the occurrence of individual events at different heights are not directly related. From bottom to top (*a*) buoyancy-production region, (*b*) convectively mixed layer, (*c*) interfacial intermittency region, and (*d*) diffusion region ($z > d_m$).

gravity waves is measured (figure 2*d*). Similar temperature records to those in figure 2 have been reported by Deardorff *et al.* (1969) and Willis & Deardorff (1974).

If the mixed layer is dyed the interface consists of a number of penetrating domes of turbulent fluid (figure 3). Penetration of the domes beyond the interface causes a net downwards displacement of fluid through the interface and hence a net downwards heat flux. Two differing theories as to the nature of the displacement mechanism have been put forward (Stull 1973; Linden 1973) but neither has been confirmed experimentally. Only the effect of the displacement process will be considered here.

It is apparent from these measurements that well above the interface there exists a profile dominated by molecular diffusivity and well below the interface there is a well-mixed turbulent region. Between the two regions there is the fluctuating boundary between the turbulent mixed layer and the diffusion region. Although the temperature at the fluctuating interface will be continuous it is expected that there will exist a sharp change in the temperature gradient between the turbulent and diffusive region. It is the exchange across this boundary which controls the movement of the interface and it

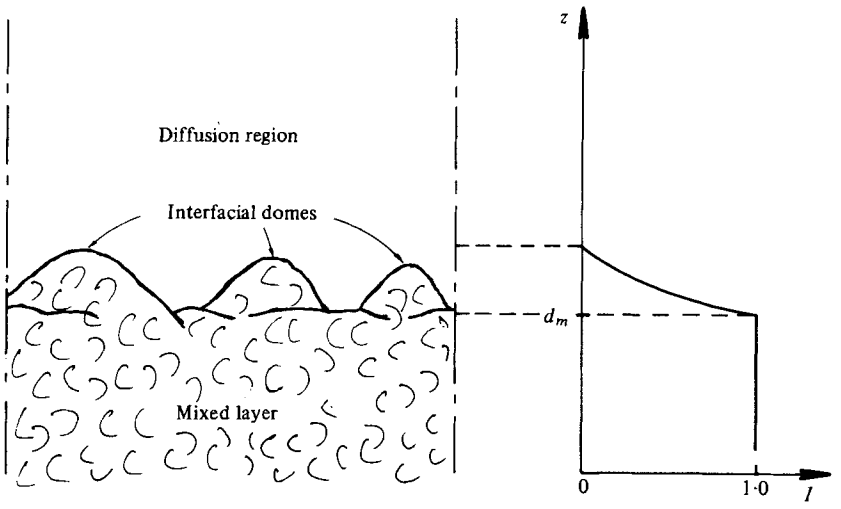

FIGURE 3. Sketch showing interfacial region between the mixed layer and diffusion region and the extent of the intermittency region $0 < I < 1$.

was thought important to preserve this boundary condition in the computational model. However for computational convenience the interface has to be taken as horizontal. It remains to determine the level of this horizontal interface.

In a particular experiment at a fixed time t and level z the area in the xy plane that is in the mixed fluid is in theory a measurable quantity. The value of this quantity will vary from unity in the mixed layer to zero in the diffusive region. If an experiment were repeated many times it should be possible to determine the ensemble average of this intermittency factor $I(z,t)$. In the numerical model the level of the equivalent horizontal interface $d_m(t)$ was taken as the highest point at which $I(z,t)$ equals unity.

At this level it is assumed that the temperature gradient is discontinuous (figure 1*a*) with a maximum temperature gradient just above the surface. Above this surface the temperature gradient decreases with increasing z until it is determined by pure diffusion.

In the real flow the turbulent heat flux and the intermittency factor also have a maximum at the interface and decrease until both go to zero where the heat flux is purely diffusive. The simplest way of matching these conditions is to express the vertical buoyancy flux for $z > d_m$ by

$$Q(z) = -(\kappa+\gamma)\partial T/\partial z, \tag{5}$$

where κ is the molecular diffusivity, and γ is a turbulent diffusivity.

To satisfy the conditions discussed above, both γ and $\partial T/\partial z$ have a maximum at the interface and γ must tend to zero when the intermittency factor tends to zero. Indeed the variation of γ with height will be closely linked to $I(z)$ (figure 3). It will be assumed that $\gamma(z)$ is described by

$$\gamma(z) = \gamma_i \phi(z-d_m) \quad \text{for} \quad z > d_m, \tag{6}$$

where $\phi(z-d_m)$ is a decay function equal to unity at the interface. The dependence of the interfacial value γ_i on the interfacial temperature gradient and on the turbulent intensity of the mixed layer will be discussed later.

Within the fluid column $0 < z < h_T$ a one-dimensional heat budget yields

$$\partial T/\partial t = -\partial Q/\partial z. \tag{7}$$

It follows from (5) and (7) that within the diffusion region ($z > d_m$)

$$\frac{\partial T}{\partial t} = \frac{\partial}{\partial z}(\kappa+\gamma)\frac{\partial T}{\partial z}. \tag{8}$$

For the isothermal mixed layer we consider the heat budget for the whole mixed layer. The heat fluxes across the two boundaries $z = 0$ and $z = d_m$ must equal the rate of increase in heat storage of the thickening mixed layer. At the lower boundary the heat input is Q_p.

Note that the interfacial heat flux, from (5), is

$$Q_e = -(\kappa+\gamma_i)(\partial T/\partial z)_i, \tag{9}$$

where $(\partial T/\partial z)_i$ is the interfacial temperature gradient (figure 1). As the heat flux is continuous at the interface, Q_e is also the heat flux transferred across the interfacial boundary into the mixed layer. From the viewpoint of an observer on the interface there is also a net flux of fluid of temperature T_m into the mixed layer at rate of v_e. This results in a heat flux of $v_e T_m$. Thus for the growing mixed layer the heat budget is

$$\frac{d}{dt}(d_m T_m) = Q_p - Q_e + v_e T_m \tag{10}$$

and therefore

$$dT_m/dt = (Q_p - Q_e)/d_m. \tag{11}$$

Now in the present model the partial derivatives of temperature with respect to height and time are assumed to be discontinuous at the interface (figure 1). As the temperature across the interface is continuous then

$$\frac{dT}{dt} = \left[\frac{\partial T}{\partial t}\right]_m = \left[\frac{\partial T}{\partial t}\right]_i + v_e\left[\frac{\partial T}{\partial z}\right]_i, \tag{12}$$

where the subscripts m and i signify values taken immediately below and above the interface. Below the interface the temperature gradient is zero. Hence

$$v_e = \left(\frac{dT_m}{dt} - \left[\frac{\partial T}{\partial t}\right]_i\right)\Big/\left[\frac{\partial T}{\partial z}\right]_i. \tag{13}$$

Substituting (8), (9) and (11) in (13) yields

$$v_{em} = \underbrace{\frac{Q_p}{d_m[\partial T/\partial z]_i}}_{\text{I}} + \underbrace{\frac{(\kappa+\gamma_i)}{d_m}}_{\text{II}} - \underbrace{(\kappa+\gamma_i)\left[\left(\frac{\partial^2 T}{\partial z^2}\right)\Big/\left(\frac{\partial T}{\partial z}\right)\right]_i}_{\text{III}} - \underbrace{\left[\frac{\partial \gamma}{\partial z}\right]_i}_{\text{IV}}. \tag{14}$$

Term I describes the rate of rise of the interface by non-penetrative convection due to the lower boundary heat flux Q_p and term II is the additional contribution due to Q_e. As will be shown later non-penetrative convection makes a significant contribution to v_e. Both terms are positive.

The effect of changes in the diffusion region profile due to molecular diffusivity, term III, may be positive or negative depending on the sign of $\partial^2 T/\partial z^2$. As γ decreases with height term IV will always be positive. Note there is a finite upper limit on v_e, which occurs for neutral conditions which is not described by (13). In mechanical

stirring-grid experiments there is no source of heat or mass, only mechanical energy, so term I is zero. Before a numerical analysis can be performed using this model equations for turbulent diffusivity $\gamma(z)$ are required.

2.1. *Turbulent diffusivity*

First consider the interfacial value γ_i. An empirical relationship for γ_i as a function of Richardson number may be obtained empirically from the high-Péclet-number stirring-grid data of Turner (1968). At high Pe, κ may be neglected and (9) yields

$$\gamma_i = -Q_e[\partial T/\partial z]_i. \tag{15}$$

Turner (1968, 1973) presented his data in the form E as a function of Ri. For the present model which includes the interfacial temperature gradient

$$E = \frac{-Q_e}{[\partial T/\partial z]_i v_s l_s}. \tag{16}$$

Therefore

$$\gamma_i = E l_s v_s. \tag{17}$$

The corresponding gradient Richardson number is

$$Ri = \alpha g[\partial T/\partial z]_i \, l_s^2/v_s^2. \tag{18}$$

The general nature of the interface when the heated fluid was dyed was indistinguishable from the author's experiments with a stirred grid in a apparatus exactly similar to that of Thompson & Turner (1975). Thompson & Turner obtained from their experiments a value of c_1 of the order 0·1 and it was therefore natural to adopt their value.

Because Turner (1968) non-dimensionalized by the interfacial temperature or salinity difference there are differences between his definition of E and (16). Interfacial measurements from later grid-stirring experiments suggest however that the interfacial thickness at large Pe is constant and of order l_s (Crapper & Linden, 1974; Hopfinger & Toly 1976). This suggests that $[\partial T/\partial z]_i$ is of the order of $\Delta T_i/l_s$ and if it is assumed that the above are equal then there is no transformation of Turner's (1968) data due to the differences in the definitions of E and Ri. However the constant c_2 in the definition of v_s (2) still needs to be evaluated. This is done indirectly in the following manner.

From (16), (18), (2) and the definition of k (4) we obtain

$$ERi = k/c^3. \tag{19}$$

As will be discussed later k is not a constant but varies with Ri (Denton 1978). Reanalysis of reported k values in terms of the present model suggests k has a maximum value of 0·2. The velocity scale constant c_2 is evaluated by fitting (19) to Turner's (1968) data such that k satisfies this value (figure 4). The resulting value of c_2 is 0·56. Using these values of c_1 and c_2 the high Pe data is best fitted by the empirical relationship (curve ABC)

$$E = \frac{1{\cdot}18}{1 + 0{\cdot}41 Ri^{\frac{3}{2}}}. \tag{20}$$

This has the form of Zilitinkevich's (1975) result but includes a $\frac{3}{2}$ power in the denominator to satisfy Turner's large Pe limit at large Ri. It provides a very good fit of the data over all Ri.

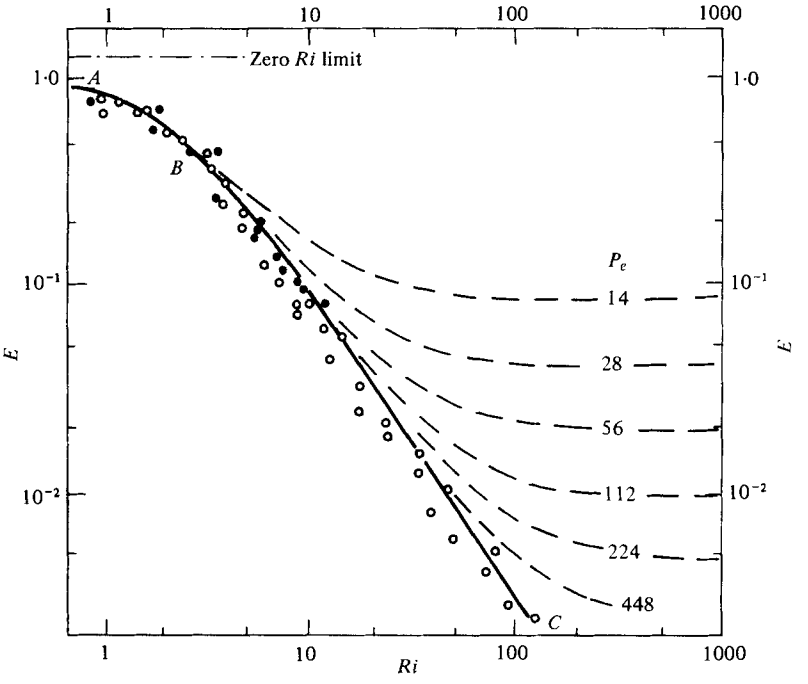

FIGURE 4. Empirical curve of ln E versus ln Ri. The (solid) curve ABC is for large Péclet number and is given by equation (20); it should be compared with Turner's experimental points. The dashed curves represent constant Péclet number. Experimental points are for salinity (○) and temperature (●).

The required empirical relationship for γ_i from (17) and (20) is

$$\gamma_i = \frac{1{\cdot}18 l_s v_s}{1 + 0{\cdot}41 Ri^{\frac{3}{2}}}. \tag{21}$$

Note that γ_i has been assumed to be independent of other factors influencing the rate of rise of the interface. If the non-penetrative convection term is large then the mixed-layer fluid rapidly becomes more buoyant than the diffusion region fluid above it. This is the same as having an unstable density stratification above the interface. In Turner's (1968) experiments there was no external source of buoyancy ($Q_p = 0$) and this problem was not encountered.

The empirical formula for E and hence γ_i differs from the previous formulae because of its $-\frac{3}{2}$ power law at high Ri. Deardorff (1974) and Zilitinkevich (1975) gave formulae which yielded a -1 power law but these are not consistent with Turner's (1968) high-Péclet-number data. An empirical formula which satisfies the same limits as (27) but a different interpolation form was suggested by Munk & Anderson (1948).

To complete the description of the turbulent transfer, the decay of $\gamma(z)$ with height must be defined. From the experimental data of Adrian (1975) and Linden (1975) this decay appears to be exponential. However to put a finite limit on the extent of γ the following power law was used in the numerical analysis

$$\gamma = \gamma_i \left(1 - \left[\frac{z - d_m}{d_i}\right]\right)^2, \tag{22}$$

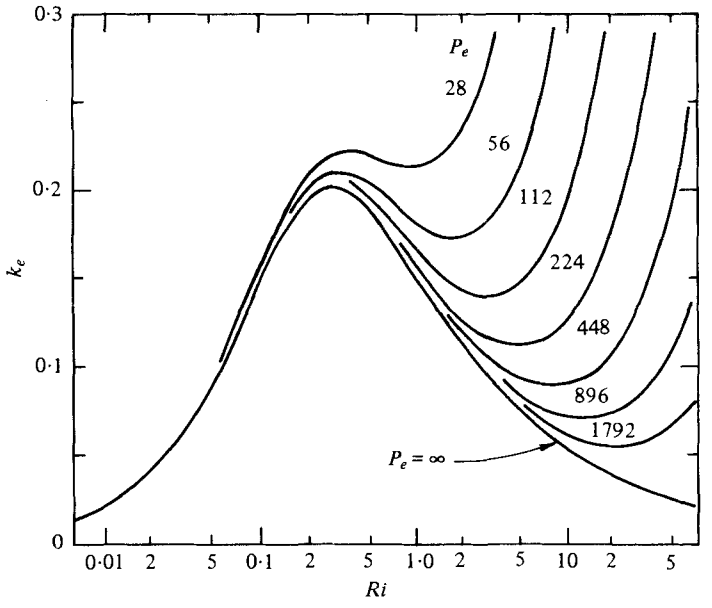

FIGURE 5. Variation of heat flux ratio k as a function of gradient Richardson number showing contours of constant Pe (from (25)).

where d_i is the thickness of the turbulent diffusion region (figure 3). From (22)

$$\left[\frac{\partial \gamma}{\partial z}\right]_i = -2\gamma_i/d_i. \tag{23}$$

The temperature gradient at the interface $[\partial T/\partial z]_i$ was assumed to be equal to $\Delta T_i/l_s$. If in a similar manner $[\partial \gamma_L/\partial z]_i$ is assumed to be equal to γ_i/l_s, then, from (23), $d_i = 2l_s$. Crapper & Linden's experiments with mechanical stirring on both sides of the interface yielded an interface thickness which was independent of the Richardson Number and was of the order of unity. This is consistent with the assumption above.

2.2. *The combined effect of turbulent and molecular diffusion*

From (9) and the high Pe definition of E (20) it follows that, for all Pe,

$$E = \frac{1{\cdot}18}{1 + 0{\cdot}41 Ri^{\frac{3}{2}}} + Pe^{-1}. \tag{24}$$

This is plotted as dashed curves in figure 4. As the Richardson number decreases, the contribution to E from turbulent diffusion increases and molecular diffusive effects become negligible (this is the same as the high Pe case). But conversely, if Ri becomes very large, turbulent diffusion is negligible and E tends to a constant value Pe^{-1}. Neither Ri nor Pe alone specify the relative effects of molecular and turbulent diffusion. Equation (24) implies that Turner's result for temperature stratification $E \propto Ri^{-1}$ is not a general law but depends on the particular experimental values of Ri and Pe. For instance at very high values of Ri his temperature data could be expected from (24) to tend to a constant E value.

Molecular diffusion also contributes to k. From (19) and (24)

$$k = \frac{0{\cdot}20Ri}{1+0{\cdot}41Ri^{\frac{3}{2}}} + \frac{0{\cdot}18Ri}{Pe}. \tag{25}$$

Figure 5 shows a plot of this relation. For stable interfaces (large Ri), k is very sensitive to Pe.

Crapper & Linden's experiments show that molecular diffusion also affects the thickness of the interface and will thus change the shape of γ. However, the average Péclet number in the experiments was 130 and the change is likely to be less than an order of magnitude. If this change is ignored then (22) and the equation for v_e (14) are now sufficient to allow temporal behaviour of this penetrative convective system to be analysed numerically.

3. Numerical analysis

To illustrate the effect of molecular diffusion at low Péclet number and the necessity for allowing an interfacial temperature gradient, the hypothetical case of no turbulent diffusion above the interface ($\gamma = 0$) will be considered first.

Figure 6 shows the results of a numerical analysis of this 'molecular entrainment' case plotted as temperature versus time with constant height contours. Details of the analysis program are given in appendix A. The initial temperatures of the two-layered stratification were 39 and 20 °C. The lower layer was 13·93 cm thick and the full fluid column 55 cm thick. Lower-boundary heating ($Q_p = 0{\cdot}023$ cal °C/s) commenced at 80 min. Fluid properties used in evaluating Ri and other terms did not vary with temperature but had values consistent with water at 20 °C. These were $\kappa = 1{\cdot}43 \times 10^{-3}$ cm^2/s, $\rho c_p = 1{\cdot}0$ cal/cm^3 °C, $\alpha = 2{\cdot}1 \times 10^{-4}$ (°C)$^{-1}$. Allowance was made for minor heat losses that occur in laboratory experiments but these did not significantly affect the temporal behaviour.

Until heating begins at $t = 80$ min there is no mixed layer and a molecular diffusion profile forms between the two layers. Even after heating begins the same molecular diffusion process continues as the effect of mixed-layer turbulence above the interface (i.e. γ) has been neglected in this analysis.

Below the interface the mixed-layer temperature is increasing owing to lower-boundary heat input and negative heat transfer by molecular diffusion through the interface (figure 6). The time when the interface reaches a given height is given by the intersection of the diffusion region temperature contour for that height and the mixed layer temperature. The resulting curve for d_m shows that the interface rises rapidly, initially when there are negligible temperature gradients, and then reduces. The lowest values of v_e occur at about $z = 14$ cm where the interfacial temperature gradients are a maximum. Later when $(\partial T/\partial z)_i$ decreases, v_e increases and the interface rises rapidly until it reaches the top of the fluid column. Thereafter single-layer convection occurs.

Also shown in figure 6 are the T_m and d_m curves for an analysis in which k is neglected after $t = 80$ min. The rate of rise of the interface in this case is only due to 'filling' of the 80 min temperature profile by lower boundary heating. This process is called non-penetrative convection. The rate of rise of the interface for molecular entrainment is much larger because of the additional interfacial heat flux and destabilizing of the fluid above the interface by molecular diffusion. Note however that initially ($80 < t$

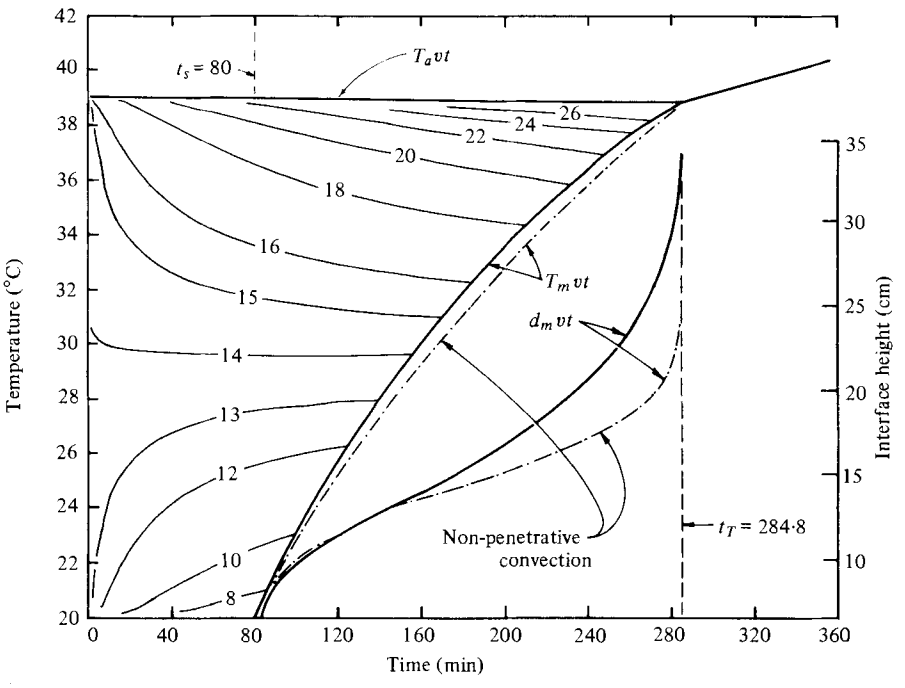

FIGURE 6. Graph of temperature versus time for molecular entrainment analysis with contours of constant height. The mixed-layer curve for the corresponding non-penetrative convection case is also shown.

< 120 min), there is an increase in temperature above the interface (stabilizing effect) which reduces v_e relative to the case in which diffusion is ignored.

Note that the molecular entrainment process can be referred to as entrainment as fluid is still transferred downwards through the interface by mixed-layer turbulence. Only the effect of this turbulence *above* the interface is neglected.

The times when the interface reaches the top of the fluid column and when $\Delta T_i \to 0$ are identical for this example (h_T = 25 cm). As the heat content of the fluid column will be the same for the analyses of both non-penetrative convection and molecular entrainment, irrespective of the internal interfacial entrainment processes, time t_T will also be the same for both. An equation for t_T is easily derived (Tennekes 1973; Denton 1978). It follows that fully turbulent entrainment ($\gamma > 0$) will give the same value of t_T. The above analysis with $\gamma = 0$ shows how the temperature changes immediately above the interface have a major effect on v_e. This is not apparent from Bett's (1973) model.

In a penetrative-convection system, however, the temperature at any given height decreases at an increasing rate as the interface reaches that height. Farmer's (1975) measurements of temperature versus time at fixed heights in an ice-covered lake (his figure 7) show this quite clearly. In the $\gamma = 0$ analysis (figure 6) the rate of change of temperature, whether positive or negative, decreases with time.

4. Comparison of numerical analyses with experimental data

The results of three numerical analyses corresponding to three experimental runs will be presented in this section. In each case the bottom heat flux ($2{\cdot}68 \times 10^{-2}$ cal/s cm^2) and fluid column height (55 cm) were the same. Initial conditions for the runs are

Experiment	ds	d_g (cm)	T_a (°C)	T_m (°C)	ΔT_i (°C)
ES1	24	10·0	40·1	17·7	22·4
ES2	36	13·9	39·2	20·5	18·7
ES3	36	23·6	38·4	10·0	28·4

TABLE 1. Initial conditions for entrainment runs.

given in table 1. The important difference between the three experiments is the initial thickness of the lower layer d_g. If d_g is small the period of interfacial entrainment is short and the temperature changes are too rapid. For larger initial values of d_g the interfacial period is much longer. However, large values of d_g relative to h_T may mean that the finite upper boundary has an influence on the later behaviour of the system.

The results of experiment ES2 will be presented first. For this experiment the interfacial entrainment period lasted about three hours. Results of the shorter experiment ES1 and the longer experiment ES3 together with their respective numerical analyses will then be discussed.

4.1. *Entrainment experiment ES2*

The results of a fully turbulent entrainment analysis of ES2 and the corresponding experimental data are shown in figure 7. Curves of mixed-layer thickness d_m versus time derived from the temperature versus time data are also plotted. The form of figure 7 is consistent with the method of data collection (appendix B). Height contours for the experimental data (dashed lines) are the best fit by eye. Limit bars on some of the data show the maximum or minimum temperature fluctuations which occurred during the fixed height reading (cf. figure 3).

The time scale of the experimental data was set to a virtual time origin by comparing the temperature profile at $t = 70$ min with the temporal development of a molecular diffusion profile having the same initial conditions. Heating commenced at $t_s = 73$ min. Because of the difficulty of accurately modelling the rate of rise of the interface when it is very large the numerical analysis began shortly after the commencement of heating at $t = 80$ min. The temperature changes before t_s are due to molecular diffusion and minor heat loss effects and are easily understood. Similarly the analysis is numerically unstable immediately prior to the interface reaching the full column height at $t = t_T$ owing to the large value of the turbulent diffusivity γ. Data at this time can be obtained by extrapolation. After $t = t_T$ when there is only one uniform layer the theory is well understood.

The initial conditions for the case in which $\gamma = 0$ were very close to those of experiment ES2 and it is therefore appropriate to compare figures 6 and 7. They show that the additional downward heat flux due to the turbulent transfer at the interface causes only a small difference in the mixed-layer temperature. (For example, at 240 min the laminar-entrainment model yields a mixed-layer temperature of 37·2 °C while the turbulent entrainment model gives 37·5 °C.) However, the same turbulent transfer causes a relatively large difference in the interfacial d_m (for example, at 240 min we get 21 and 25 cm respectively for the laminar and turbulent entrainment models).

Before discussing the ability of the computational model to simulate the experimental data other forms of plotting the data will be presented. These will further

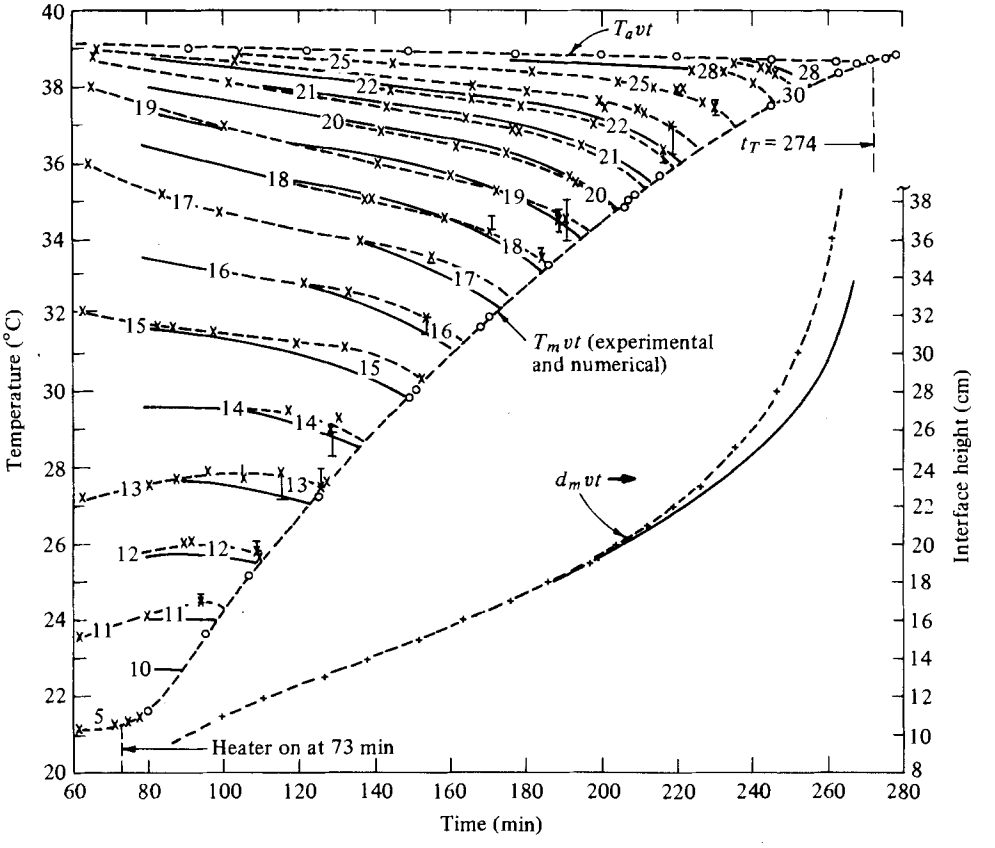

FIGURE 7. Temperature versus time plot for ES2 showing experimental data (dashed curve) and numerical analysis (solid curve) commencing at $t = 80$ min. Contour labels give height in centimetres. Also plotted is interface height as a function of time.

illustrate the way changes in the temperature above and below the interface interact and allow the convection layer to grow.

Vertical temperature profiles from the numerical analysis of ES2 and derived from the experimental data are shown in figures 8 (*a*) and (*b*). The locus of d_m and T_m values is useful in defining the interface height when d_m is not an integer centimetre value. The locus also represents a minimum temperature envelope. For non-penetrative convection it is the same as the temperature depth profile at the start of heating ($t = t_s$) (neglecting minor heat losses). When the effect of molecular and turbulent diffusion above the interface is included there is substantial diffusion-region cooling allowing the interface to rise further.

To obtain profiles of buoyancy heat flux from the experimental data the following method is used (figure 9). A heat budget for a horizontal section of the insulated fluid column yields

$$\frac{\partial Q}{\partial z} = -\beta \frac{\partial T}{\partial t} - W(T - T_{\text{air}}), \tag{26}$$

where β is a factor slightly greater than unity which accounts for the additional heat storage capacity of the walls and insulation, W is the heat loss factor for the walls

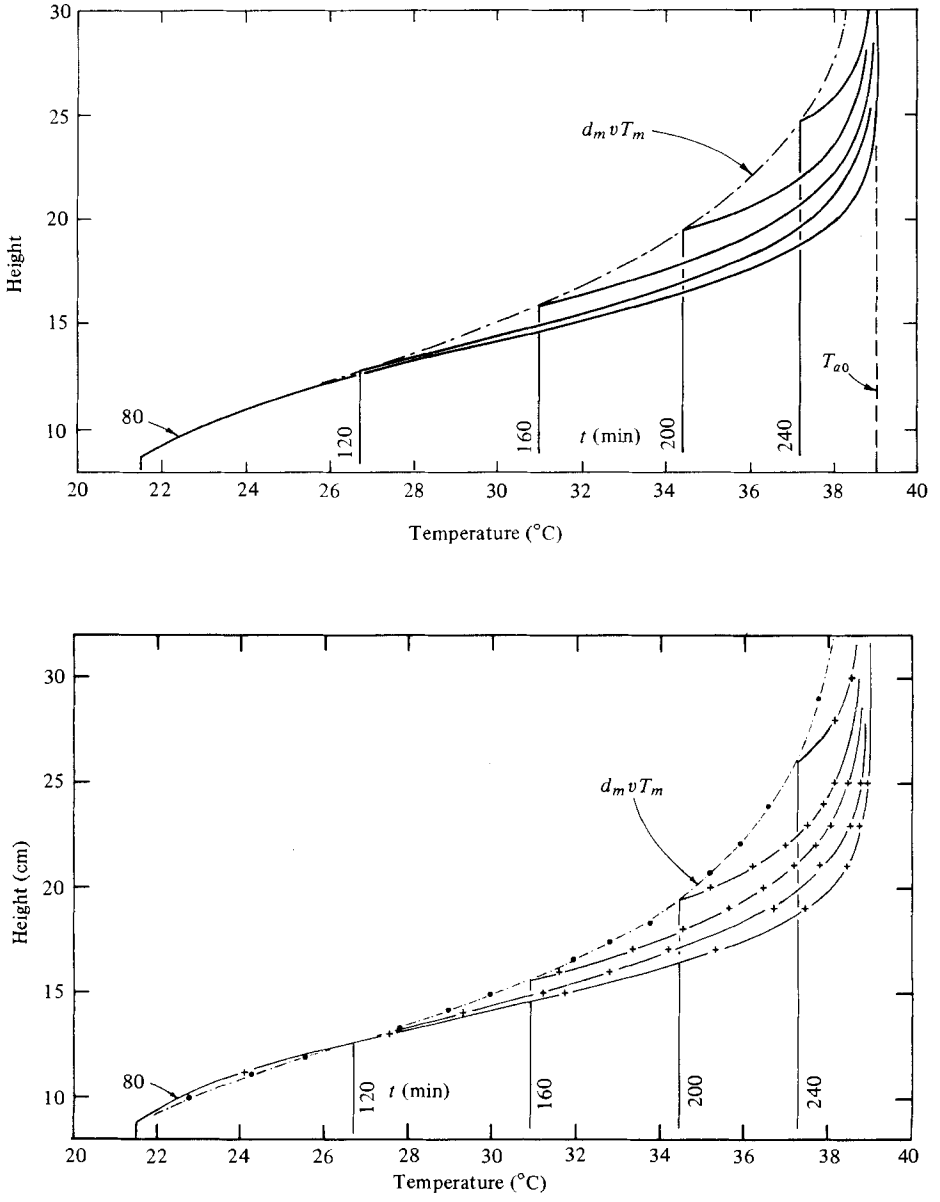

FIGURE 8. Temperature profiles from (*a*) numerical analysis of ES2 and (*b*) experimental data, with locus of mixed-layer thickness and temperature. Profile labels give time in minutes. +, $z > d_m$; ●, $z = d_m$.

and T_{air} is a representative external air temperature. Integrating (26) with respect to height from $z = 0$ to z,

$$Q(z) = Q_p - \beta \int_0^z \frac{\partial T}{\partial t} dz - W \int_0^z (T - T_{\text{air}}) dz. \tag{27}$$

Evaluating the second term on the right-hand side of the equation requires integrating the vertical profile of the partial derivative of temperature with respect to time $\partial T/\partial t$

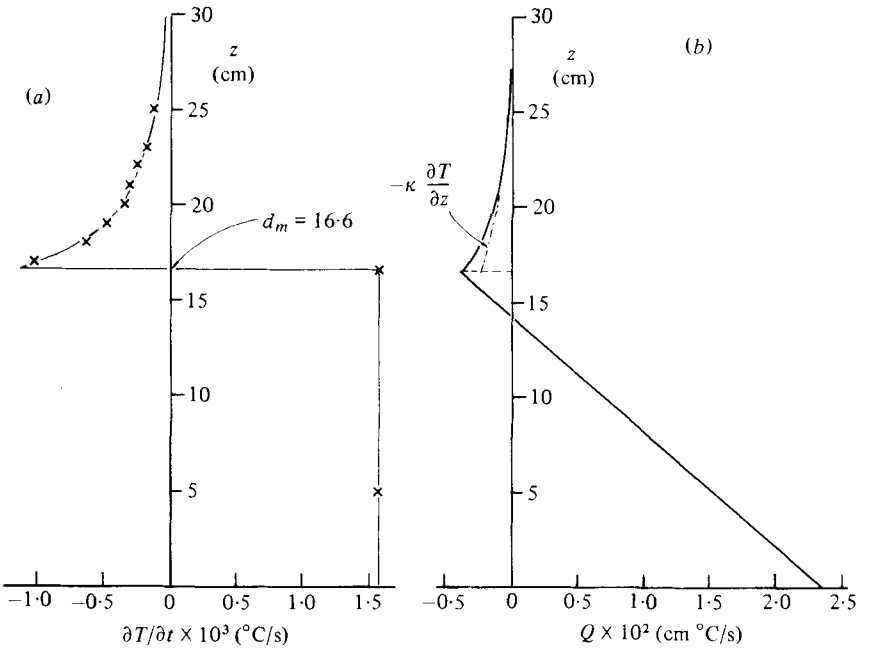

FIGURE 9. (*a*) Vertical profile of the partial derivative of temperature with respect to time from experiment ES2 at t = 170 minutes; (*b*) buoyancy heat-flux profile derived from it.

(figure 9). This $\partial T/\partial t$ profile is obtained from the slopes of the constant height contours at a given time (in this case t = 170 min). This integration was evaluated using Simpson's rule. The third term in (27) is integrated in a similar way from the vertical profile of temperature (figure 8*b*).

The resulting profile of buoyancy heat flux for ES2 at t = 170 min is shown in figure 9(*b*). The heat-flux curve due to molecular diffusion above the interface ($-\kappa \partial T/\partial z$) is also plotted. It is of interest to note that the experimental value of $k = -Q_e/Q_p$ is 0·17. A significant portion of this value (77 %) is due to molecular diffusion. The experimental values of d_m, Q_p and $(\partial T/\partial z)_i$ with equations (11), (17) and (1) give Ri = 92·9 and Pe = 129. Substituting these values into (25) yields k = 0·18. Considering the degrees of uncertainty in the experimental data and empirical equation for $E(Ri)$ these two values are in good agreement.

It is important to note that Deardorff *et al.* (1969) obtained vertical buoyancy heat-flux profiles by integrating the time-averaged temperature changes between successive temperature profiles. However, because of the discontinuity in $\partial T/\partial t$ this method underestimates the heat fluxes in the region of the interface (Cattle & Weston 1975; Denton 1978). The first check on the ability of the numerical analysis to simulate the experimental ES2 data is the behaviour of $T_m(t)$ (figure 7). In a cooling pond the heat loss to the atmosphere is a function of the temperature difference between T_m and the air. In this example the agreement is extremely good. However, this check is not very sensitive. Any overestimation of the interfacial flux Q_e will mean a corresponding overestimation of the interface height d_m. The extra heat transferred through the interface will be distributed over a thicker mixed layer and the resulting error in T_m will be small.

The second check is the interface height $d_m(t)$. Although not such a major factor in

cooling ponds the rate of growth of the mixed layer is important in atmospheric modelling. For experiment ES2 d_m is modelled well up to $t = 220$ min. For the remaining portion of the experiment the computed depth at any time underestimated the real depth. As T_m is accurately predicted these errors are due to errors in the diffusion. The changes in temperature here are given by

$$\frac{\partial T}{\partial t} = \frac{1}{\beta}\frac{\partial}{\partial z}(\kappa+\gamma)\frac{\partial T}{\partial z} - \frac{W}{\beta}(T - T_{\text{air}}), \tag{28}$$

where, as in (26), β and W are included to account for minor heat-loss effects. The temperature changes are very sensitive to the values of γ and $\partial\gamma/\partial z$. However, as there is good agreement up to 220 min the empirical formulae for $\gamma(z)$ appear to be able to successfully model turbulent entrainment effects where the interfacial gradient is large.

Next it is appropriate to compare the temperature time contours at each fixed depth. There is general agreement between computed and measured depth contours on the temperature time graph (figure 7). The only poor agreement in the shape of curves is for the contours at $z = 11$, 12 and 13 cm. These increase with time, only cooling when the interface is within 1 cm of the given height (figure 7). In the numerical analysis the temperatures decrease much sooner, suggesting $\gamma(z)$ is overestimated. This reduction in $\gamma(z)$ in the experimental case could be due to the filling velocity or non-penetrative convection effect discussed earlier. If d_m is small, T_m increases rapidly and hence rapidly destabilizes the interface. Thermal elements penetrating above the rapidly rising interface will have less effect on the diffusion-region fluid (i.e. $z > d_m$) and hence $\gamma(z)$ is reduced. Note that, as the mixed layer rises, diffusion region just above d_m is incorporated into the mixed layer and cumulative errors here are removed from consideration.

It is expected that the major reason for the inadequacy of the numerical predictions when t is greater than 220 min is the very small ΔT_i in this region. This implies that the buoyancy forces are small and the penetrating domes remain in the diffusion region. Thus the interface rises rapidly and the turbulent diffusion parameter concept breaks down.

4.2. *Entrainment experiment ES3*

In this experiment the initial value of d_g was relatively large (22 cm) and the values of d_m and T_m increase more slowly. The rapid non-penetrative convection effect discussed above is not significant and the initial agreement of the diffusion region temperatures ($z < d_g$) is reasonable (figure 10). It also follows that the magnitude of γ_i should be generally lower than for experiment ES2 as the mixed-layer thickness is correspondingly higher. Both l_s and Ri are higher and hence E and γ_i are smaller. The mixed-layer height prediction agrees well with the experimental data especially up to $t = 250$ min. As this experiment is much longer, cumulative heat-loss effects should be much more significant. Note experiment ES3 was stopped after 5·5 h of heating when the interface height was 38 cm and the diffusion region thickness was only 17 cm.

4.3. *Entrainment experiment ES1*

This experiment with its relatively small value of the initial cold-layer thickness d_g (10 cm) shows quite clearly the effect of non-penetrative convection (figure 11). The

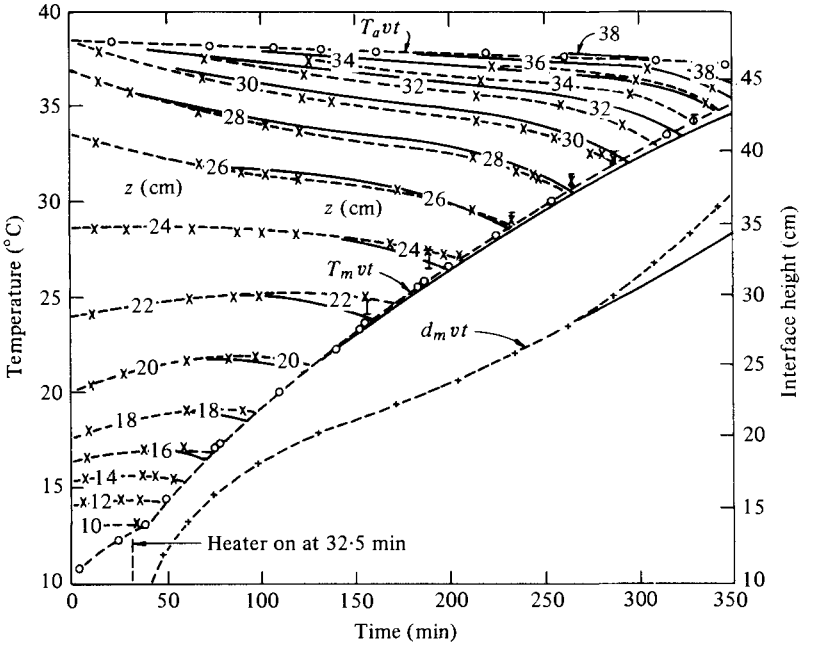

FIGURE 10. Temperature versus time plots for ES3 from experimental data (dashed curve) and numerical analysis (continuous curve). Contour labels give height in centimetres. Interface height as function of time is also plotted.

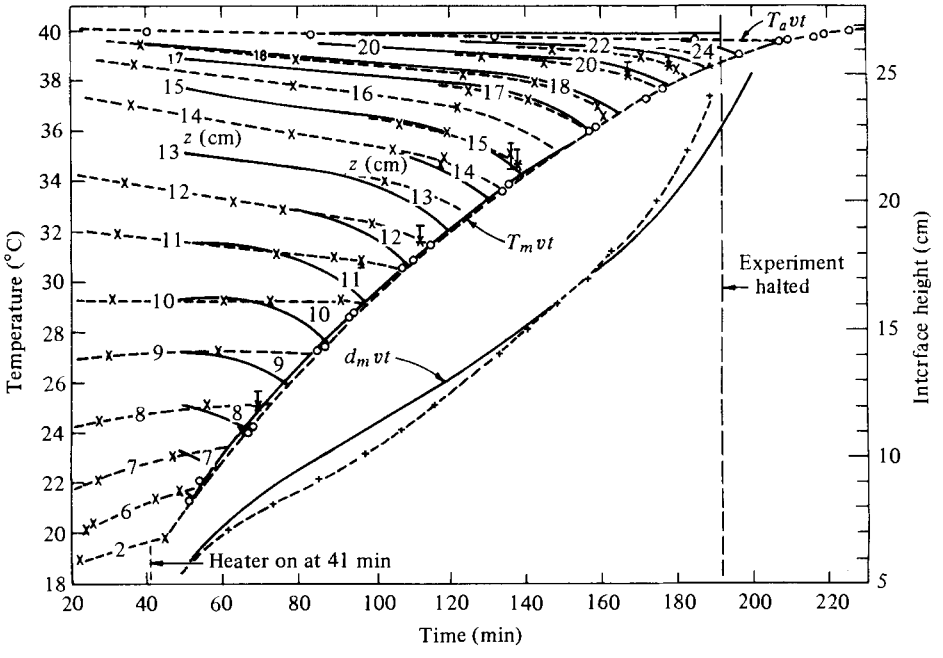

FIGURE 11. Temperature versus time plots for ES1 from experimental data (dashed curve) and numerical analysis (continuous curve). Contour labels give height in centimetres. Interface height as a function of time is also plotted.

empirical formula for $\gamma(z)$ in the numerical model predicted large values of γ_i because d_m is correspondingly smaller but the experimental temperatures at constant height ($z > d_m$) do not appear to be substantially affected by the penetrating interfacial domes. Instead the temperatures vary in the manner of a molecular entrainment analysis in which $\gamma = 0$. Only after $t = 100$ min do turbulent diffusion effects become significant. This is presumably due to the importance of the non-penetrative convection term. However, as expected there is generally poor agreement between the diffusion region temperatures and mixed-layer heights d_m (figure 11).

5. Conclusions

A penetrative-convection model which allows for molecular diffusion at low Péclet number has been developed. The model assumes a discontinuity in the partial derivatives of temperature with respect to height and time at the interface while allowing the temperature and buoyancy heat flux to be continuous.

The additional heat transfer due to the penetration of interfacial domes of turbulent convection-layer fluid was parameterized by a turbulent diffusivity term γ acting on the interfacial gradient. The empirical relationship obtained for this term relates two previous methods of presenting interfacial entrainment data. The use of a gradient Richardson number based on the interfacial temperature gradient rather than the temperature difference across the interface enables the two methods to be combined into a single equation. This explains the variation of Turner's (1968, 1973) data with the Péclet and Richardson numbers and the variation of the heat flux ratio k.

Non-penetrative convection due to the 'filling' of the existing temperature profile relative to the interfacial temperature gradient can amount to as much as one-half of the rate of rise of the interface. Similarly the contribution by molecular diffusion may be of the same order of magnitude as that by turbulent diffusion. These quantities show the importance of including the interfacial temperature gradient in the model.

Three experimental runs have been used to check the numerical analysis results. Good agreement has been found. However a wider range of data is needed. In particular the formula for turbulent diffusivity should be tested using high-Péclet-number data. Improvements to the numerical model would include an allowance for the following. (1) The variation in α and the molecular diffusivity κ with temperature. (2) The reduced effect above the interface of the penetrating interfacial domes when the mixed layer temperature is rapidly rising. The rapid destabilizing of the interface causes the turbulent diffusion parameter γ derived from experimental data to be smaller than that predicted by the empirical formula. (3) A change in the interface thickness at low Péclet numbers (Crapper & Linden 1974).

Financial assistance for this research was provided by the New Zealand Electricity Department and the University Grants Committee of New Zealand. Some of the initial preparation of this paper was carried out while the first author was employed by the New Zealand Oceanographic Institute and completed during his present employment by Sonderforschungsbereich 80, University of Karlsruhe, West Germany.

Appendix A. Numerical computer program

The numerical analyses were carried out on the University of Canterbury's Burroughs B6718 computer. In the turbulent entrainment analysis program, diffusion region temperature changes were calculated first. The diffusion region was represented by a vertical array of equally spaced finite-difference nodes extending from $z = h_T$ down to a point immediately below the existing interface. A forward-difference scheme was then used to calculate the temperature changes. A more sophisticated scheme was not possible because the diffusion region ($z > d_m$) is only weakly controlled by the mixed-layer conditions (through the turbulent diffusivity $\gamma(z)$) and hence is effectively unbounded at $z = d_m$. The temperature change of the lowest node (immediately below the interface) was obtained by fitting the temperature changes of the five nodes above with a simplified cubic equation ($ax^3 + bx + c$) and extrapolating.

It was unfortunate that the temperature gradient at the interface, the region of most interest, and the controlling factor for the rate of growth of the mixed layer had to be calculated by extrapolation. However the good agreement between the experimental and numerical results suggest this computing method was acceptable.

Once the new diffusion-region temperatures were known, changes in mixed-layer temperature and height were calculated from changes in the mixed-layer heat budget over the time increment δt. As it generally required of order 10^2 time steps for the interface to rise between a pair of finite-difference nodes, a linear interpolation of the temperature between each pair of nodes was necessary. Heat losses were included in the temperature change calculations but the variation of the fluid properties with temperature was ignored. As κ and α vary significantly over the temperature range 20 °C $< T <$ 40 °C this simplification will affect the temperature change calculation.

Molecular entrainment analyses could be performed by merely setting $\gamma = 0$. However as the diffusion region is completely independent of the mixed layer when $\gamma = 0$ an analytical solution of the diffusion-region temperature profile was also possible. From the known temperature conditions at the existing interface height and (10) the rate of rise of the interface v_e could be calculated and the new interface height obtained using forward differences (i.e. $d_m = d_m + v_e \delta t$). Substituting the new interface height into the diffusion-region temperature profile equation yielded the new mixed-layer tem perature T.

Appendix B. Experimental investigation

The fluid column was contained within an insulated Perspex tank, 30 cm square and 55 cm deep. Two-layer temperature stratifications were formed by partly filling the tank with warm water and then feeding in cold water through a 0·16 cm gap at the base of one of the side walls. Owing to inflow mixing and molecular diffusion a diffusion profile with a thickness of order 10 cm usually resulted between the two layers.

Following Krishnamurti (1970) the lower boundary heat flux was held constant by controlling the temperature drop across a poor thermal conductor (a glass sheet, 30 cm square and 0·217 cm thick, typical thermal conductivity $2{\cdot}3 \times 10^{-3}$ cal/s cm °C) sandwiched between two plates. The upper plate was machined from aluminium alloy to a thickness of 2·34 cm. Its plan dimensions matched the exterior of the Perspex tank (32·8 cm square). The lower block of 7·3 cm thick case aluminium contained a 1000 W length of resistance heating.

The heat input was controlled by a thermopile consisting of eight chromel–alumel thermocouples mounted alternately above and below the glass sheet and linked in series. The output was linked to a control circuit which maintained a constant temperature drop across the glass by on–half-on–off switching of the heater. An additional variable load resistor was used to tune the system so that the heater switched off infrequently. Because of the heat capacity of the upper aluminium plate the heat flux into the fluid column q_p was weakly dependent upon the rate of rise of mixed-layer temperature. This was allowed for in analysing the data.

Vertical temperature profiles were obtained using a rapid response chromel–alumel thermocouple probe. A manual traversing system was used to enable regions of greatest temperature variation (i.e. immediately above the interface) to be sampled more frequently. Moving the probe was found to cause damped buoyancy oscillations in the fluid. The probe was always brought to rest for 10–20 s before a reading was taken. Note that, when the interface is not perfectly horizontal, horizontal averaging will obscure the interfacial discontinuity. A horizontally averaging probe of the type used by Deardorff *et al.* (1969) was therefore discounted. Additional fixed thermocouples were mounted in the sides of the tank.

Inaccurate height settings for the probe can lead to large temperature errors, for example, for $\partial T/\partial z = 1$ °C/cm, a height error of only 0·1 cm will yield a 0·1 °C temperature error. However the large temperature fluctuations occurring in the mixed layer and above the interface (figure 3) were often of greater magnitude than the accuracy of the temperature measurement system. The problems of discerning between the undisturbed fluid temperature and the temperature due to the presence of a thermal element were greater sources of error. As each temperature reading took about 30 seconds the data is insufficient to accurately derive the rates of temperature variations. A large number of continuously reading sensors would be an obvious improvement but would cause too much flow disturbance.

REFERENCES

Adrian, R. J. 1975 Turbulent convection in water over ice. *J. Fluid Mech.* **69**, 753–781.

Betts, A. K. 1973 Non-precipitating cumulus convection and its parameterization. *Quart. J. Roy. Met. Soc.* **99**, 178–196.

Cattle, H. & Weston, K. J. 1975 Budget studies of heat flux profiles in the convection boundary layer over land. *Quart. J. Roy. Met. Soc.* **101**, 353–363.

Crapper, P. F. & Linden, P. F. 1974 The structure of turbulent density interfaces. *J. Fluid Mech.* **65**, 45–63.

Deardorff, J. W. 1970 Convective velocity and temperature scales for the unstable planetary boundary layer and for Rayleigh convection. *J. Atmos. Sci.* **27**, 1211–1213.

Deardorff, J. W. 1974 Three-dimensional numerical study of the height and mean structure of a heated planetary boundary layer. *Boundary Layer Met.* **7**, 81–106.

Deardorff, J. W., Willis, G. E. & Lilly, D. K. 1969 Laboratory investigation of non-steady penetrative convection. *J. Fluid Mech.* **35**, 7–31.

Denton, R. A. 1978 Entrainment by penetrative convection at low Péclet Number. *Dept Civil Engng, Univ. Canterbury, Christchurch, N.Z.*, rep. no. 78/1.

Denton, R. A. & Wood, I. R. 1974 Convective motions and resulting entrainment in a two-layered fluid system heated from below. *Conf. on Hydraulics and Fluid Mech., Christchurch, N.Z.*, vol. III, pp. 361–368.

FARMER, D. M. 1975 Penetrative convection in the absence of mean shear. *Quart. J. Roy. Met. Soc.* **101**, 869–891.

HEIDT, F. D. 1977 The growth of a mixed layer in a stratified fluid. *Boundary Layer Met.* **12**, 439–461.

HOPFINGER, E. J. & TOLY, J. A. 1976 Spatially decaying turbulence and its relation to mixing across density interfaces. *J. Fluid Mech.* **78**, 155–175.

HOWARD, L. N. 1964 Convection at high Rayleigh number. *Proc. 11th Int. Cong. Appl. Mech., Munich* (ed. H. Görtler), pp. 1109–1115. Berlin: Springer.

KRISHNAMURTI, R. 1970 On the transition to turbulent convection. 1. The transition from two to three dimensional flow. *J. Fluid Mech.* **42**, 295–307.

LINDEN, P. F. 1973 The interaction of a vortex ring with a sharp density interface: a model for turbulent entrainment. *J. Fluid Mech.* **60**, 467–480.

LINDEN, P. F. 1975 The deepening of a mixed layer in a stratified fluid. *J. Fluid Mech.* **71**, 385–405.

MUNK, W. H. & ANDERSON, E. R. 1948 Notes on a theory of the thermocline. *J. Marine Res.* **7**, 276–295.

ROUSE, H. & DODU, J. 1955 Diffusion turbulence à travers une discontinuité de densité. *La Houille Blanche* **10**, 522–532.

SPARROW, E. M., HUSAR, R. B. & GOLDSTEIN, R. J. 1970 Observations and other characteristics of thermals. *J. Fluid Mech.* **41**, 793–800.

STULL, R. B. 1973 Inversion rise model based on a penetrative convection. *J. Atmos. Sci.* **30**, 1092–1099.

STULL, R. B. 1976 The energetics of entrainment across a density interface. *J. Atmos. Sci.* **33**, 1260–1267.

TENNEKES, H. 1973 A model for the dynamics of the inversion above a convective boundary layer. *J. Atmos. Sci.* **30**, 558–567.

THOMPSON, S. & TURNER, J. S. 1975 Mixing across an interface due to turbulence generated by an oscillating grid. *J. Fluid Mech.* **67**, 349–368.

TOWNSEND, A. A. 1964 Natural convection in water over an ice surface. *Quart. J. Roy. Met. Soc.* **90**, 248–259.

TURNER, J. S. 1968 The influence of molecular diffusivity on turbulent entrainment across a density interface. *J. Fluid Mech.* **33**, 639–656.

TURNER, J. S. 1973 *Buoyancy effects in fluids.* Cambridge University Press.

WILLIS, G. E. & DEARDORFF, J. W. 1974 A laboratory model of the unstable planetary boundary layer. *J. Atmos. Sci.* **31**, 1297–1307.

WOLANSKI, E. J. & BRUSH, L. M. 1975 Turbulent entrainment across stable density step structures. *Tellus*, **27**, 259–268.

ZILITINKEVICH, S. S. 1975 Comments on a 'A Model for the dynamics of the inversion above a convective boundary layer'. *J. Atmos. Sci.* **32**, 991–992.